

Resonant tunneling and Fano resonance in quantum dots with electron-phonon interaction

Akiko Ueda and Mikio Eto

*Faculty of Science and Technology, Keio University,
3-14-1 Hiyoshi, Kohoku-ku, Yokohama 223-8522, Japan*

(Dated: September 19, 2018)

Abstract

We theoretically study the resonant tunneling and Fano resonance in quantum dots with electron-phonon (e-ph) interaction. We examine the bias-voltage (V) dependence of the decoherence, using Keldysh Green function method and perturbation with respect to the e-ph interaction. With optical phonons of energy ω_0 , only the elastic process takes place when $eV < \omega_0$, in which electrons emit and absorb phonons virtually. The process suppresses the resonant amplitude. When $eV > \omega_0$, the inelastic process is possible which is accompanied by real emission of phonons. It results in the dephasing and broadens the resonant width. The bias-voltage dependence of the decoherence cannot be obtained by the canonical transformation method to consider the e-ph interaction if its effect on the tunnel coupling is neglected. With acoustic phonons, the asymmetric shape of the Fano resonance grows like a symmetric one as the bias voltage increases, in qualitative accordance with experimental results.

PACS numbers: 71.38.-k, 73.21.La, 73.23.-b

I. INTRODUCTION

In semiconductor quantum dots, preservation of quantum coherence is an important issue for the application to the quantum information processing. To examine the coherence, the transport measurements have been reported using an Aharonov-Bohm (AB) ring with an embedded quantum dot, as an interferometer.^{1,2,3} The AB oscillation of the current has been observed as a function of magnetic flux penetrating the ring. The conductance usually shows a Breit-Wigner resonance of symmetric Lorentzian shape, as a function of gate voltage which changes the electrostatic potential in the quantum dot.^{1,2} This indicates that electrons pass by a discrete level in the quantum dot coherently by the resonant tunneling. The transmitted wave of the electrons interferes with the wave traversing the other arm of the ring (reference arm), which results in the AB oscillation.⁴

When the higher-order interference between the waves is important, the resonant shape is modified. Kobayashi *et al.* have observed an asymmetric peak of the conductance, as a function of the gate voltage.³ This is ascribable to the Fano resonance, which is generally caused by the interference between a discrete level and the continuum of states.⁵ The Fano resonance is observable when the wave through a discrete level interacts with the wave traversing the reference arm sufficiently before it goes out of the ring: A naive picture in the path integral formalism is as follows. An incident wave from the source is split into two arms, one includes a quantum dot and the other is the reference arm, and meets at the other side of the ring. Some part of the wave goes out to the drain and the rest goes back to the original point along both arms and interacts, and so forth. If the phase relaxation length, l_ϕ , is comparable with the size of the ring, the shortest paths dominantly contribute to the current and result in the AB oscillation. Then we observe the Breit-Wigner resonance, as a function of gate voltage, which reflects the amplitude of a wave through the quantum dot. If l_ϕ is much larger than the ring size, the contribution from many paths modifies the resonant shape to the Fano resonance; an asymmetric shape with peak and dip is produced by positive or negative interference on either side of the Breit-Wigner resonance where the phase shift differs by π from each other. In Ref. 3, the asymmetric shape of the current becomes a symmetric one when the bias voltage increases. This implies that the finite bias significantly reduces l_ϕ .

The resonances in the AB interferometer have been theoretically studied by several

groups.^{6,7,8,9,10,11,12,13,14,15,16} The electron-electron interaction has been investigated, which leads to the “Fano-Kondo effect.”^{8,10} Few theoretical work, however, has been done for the decoherence in the transport under a finite bias. In our previous paper, we have considered the dephasing effect in the reference arm phenomenologically on the Fano resonance.¹³ The dephasing effect on the AB oscillation by the spin-flip has been studied (in the case of Breit-Wigner resonance) when an odd number of electrons are localized in the quantum dot.^{6,9}

In the present paper, we examine the decoherence in the resonances by the electron-phonon (e-ph) interaction. Although the e-ph interaction in quantum dots has been studied by several groups,^{17,18,19,20,21,22,23,24,25} the bias-voltage dependence has not been clarified even in the Breit-Wigner resonance. Hence we discuss the e-ph interaction under a finite bias in the Breit-Wigner resonance as well as in the Fano resonance. The aims and main results of our study are as follows.

(i) First of all, we study the effects of longitudinal optical phonons on the Breit-Wigner resonance. To calculate the current under a finite bias, we adopt the Keldysh Green function method^{26,27} and consider the e-ph interaction by the perturbation expansion.^{17,18} Within the second-order perturbation, we distinguish elastic and inelastic processes at zero temperature. When the bias voltage is smaller than the phonon energy ω_0 , only the elastic process takes place, in which electrons virtually emit and absorb phonons. This process does not cause the dephasing, but it suppresses the resonant peak height without any change of the peak width. When the bias voltage is larger than ω_0 , an inelastic process is possible, in which electrons actually emit phonons. This results in the dephasing²⁴ and broadens the peak width.

(ii) In some papers,^{19,20,23,28} the e-ph interaction is treated by the canonical transformation method, in which e-ph interaction is considered exactly in the quantum dot, whereas its effect on the tunnel coupling is disregarded. We calculate the Breit-Wigner and Fano resonances with optical phonons by the method. By comparison with the perturbation calculation, we find some problems with the canonical transformation method to obtain the bias-voltage dependence.

(iii) We examine the effects of acoustic phonons on the Breit-Wigner resonance and Fano resonance. For the purpose, we extend the self-consistent Born approximation to the finite-bias transport in the Keldysh Green function formalism.^{17,18} We find strong suppression of

the peak height in the Breit-Wigner resonance since both elastic and inelastic processes are possible even at low bias in the case of acoustic phonons. In the Fano resonance, we show that the asymmetric shape is significantly influenced so that the dip almost disappears. This is in qualitative agreement with the experimental results.³

Concerning (i), Marquardt and Bruder have studied the elastic and inelastic processes in sequential tunneling through two quantum dots in parallel (double-dot interferometer).²⁴ They have discussed “renormalization effect” in the elastic process and “dephasing” in the inelastic process. The former stems from the difference between the ground state of an environment in the presence or absence of an electron in the quantum dots. The effect reduces the effective tunnel coupling between the quantum dots and leads. This is not the case in our resonant tunneling in which an electron virtually stays in a quantum dot, with emitting and absorbing phonons, in the elastic process. We do not find the reduction of the peak width, whereas the zero-point fluctuation of the phonons decreases the resonant peak height.

The organization of the present paper is as follows. In Sec. II, we present our model for the AB interferometer with an embedded quantum dot. The expression of the current is derived in terms of the retarded Green function. Section III is devoted to the explanation of how to treat the e-ph interaction in the Keldysh Green function formalism. The calculated results with optical phonons are shown in Sec. IV, whereas those with acoustic phonons are given in Sec. V. The conclusions are presented in Sec. VI.

II. MODEL AND CALCULATION METHOD

A. Model

Our model for the AB interferometer is shown in Fig. 1. There are two paths between leads L and R, one path connects the leads through a quantum dot by t_L and t_R , and the other path connects the leads directly by $W e^{i\varphi}$ (reference arm). The phase φ represents the magnetic flux in the ring. The bias voltage between the leads is given by $eV = \mu_L - \mu_R$, where μ_L (μ_R) is the chemical potential in lead L (R). We fix $\mu_L = eV$ and $\mu_R = 0$. Omitting

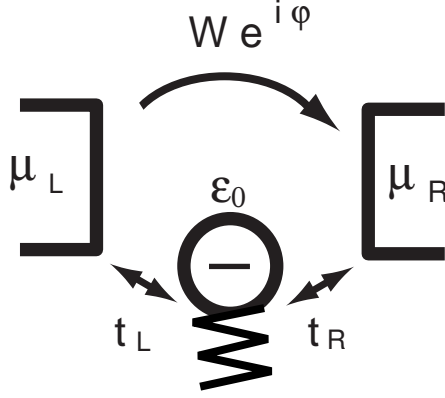


FIG. 1: Model that we adopt for an AB ring with an embedded quantum dot in the presence of electron-phonon interaction inside the quantum dot. The phase φ represents the magnetic flux in the ring.

the spin indices, the Hamiltonian for electrons is written as

$$H_{\text{el}} = H_L + H_R + H_T + H_D, \quad (1)$$

$$H_{L(R)} = \sum_k \varepsilon_k c_{L(R)k}^\dagger c_{L(R)k}, \quad (2)$$

$$H_D = \varepsilon_0 d^\dagger d, \quad (3)$$

$$\begin{aligned} H_T = & \sum_k (t_L c_{Lk}^\dagger d + \text{H.c.}) \\ & + \sum_k (t_R c_{Rk}^\dagger d + \text{H.c.}) \\ & + \sum_{kk'} (W e^{i\varphi} c_{Rk'}^\dagger c_{Lk} + \text{H.c.}), \end{aligned} \quad (4)$$

where $c_{L(R)k}^\dagger$ and $c_{L(R)k}$ denote the creation and annihilation operators of electron with momentum k in lead L (R), respectively. We assume a single energy level ε_0 in the quantum dot, with creation and annihilation operators being d^\dagger , d . The electron-electron interaction is neglected.

The strength of the tunnel coupling between the quantum dot and leads is characterized by the level broadening, $\Gamma = \Gamma_L + \Gamma_R$ with $\Gamma_{L(R)} = 2\pi t_{L(R)}^2 \nu$, where ν is the density of states in the leads. We define $\xi = \pi^2 \nu^2 W^2$ for the direct tunnel coupling between the leads. The transmission probability through the reference arm is given by $T_r = 4\xi/(1+\xi)^2$. We examine the Breit-Wigner resonance without the reference arm by choosing $\xi = 0$ and Fano-resonance by $\xi \neq 0$.

We consider the e-ph interaction inside the quantum dot. The Hamiltonian for the interaction and that for the phonons are given by

$$H_{\text{e-ph}} = \sum_{\mathbf{q}} M_{\mathbf{q}}(a_{\mathbf{q}} + a_{-\mathbf{q}}^{\dagger})d^{\dagger}d, \quad (5)$$

$$H_{\text{ph}} = \sum_{\mathbf{q}} \omega_{\mathbf{q}} a_{\mathbf{q}}^{\dagger} a_{\mathbf{q}}, \quad (6)$$

respectively, where $a_{\mathbf{q}}^{\dagger}$ ($a_{\mathbf{q}}$) creates (annihilates) a phonon with momentum \mathbf{q} . Unless otherwise noted, we will be setting \hbar to unity. The coupling coefficient $M_{\mathbf{q}}$ is written as

$$M_{\mathbf{q}} = \lambda_{\mathbf{q}} \langle d | e^{i\mathbf{q}\cdot\mathbf{r}} | d \rangle, \quad (7)$$

with $\lambda_{\mathbf{q}}$ being the amplitude of the e-ph interaction in the two dimensional electron gas. $|d\rangle$ represents the envelope function of electrons in the quantum dot. It should be noted that the electron-phonon interaction is negligibly small when $|\mathbf{q}| \gtrsim 2\pi/L$, where L is the size of the dot, owing to an oscillating factor of $\langle d | e^{i\mathbf{q}\cdot\mathbf{r}} | d \rangle$. Hence we can restrict the summation over \mathbf{q} to be $|\mathbf{q}| \lesssim 2\pi/L$ in Eqs. (5) and (6).

The current is expressed as [see Appendix A]

$$\begin{aligned} I = & \frac{2e}{h} \int d\omega [f_L(\omega) - f_R(\omega)] \\ & \times \left\{ T_r + \sqrt{\alpha T_r(1 - T_r)} \tilde{\Gamma} \cos \varphi \text{Re} G_{\text{dd}}^r(\omega) \right. \\ & \left. - \frac{1}{2} [\alpha(1 - T_r \cos^2 \varphi) - T_r] \tilde{\Gamma} \text{Im} G_{\text{dd}}^r(\omega) \right\}, \end{aligned} \quad (8)$$

where $G_{\text{dd}}^r(\omega)$ is the Fourier transform of the retarded Green function of the quantum dot,

$$G_{\text{dd}}^r(t - t') = -i\theta(t - t') \langle \{d(t), d^{\dagger}(t')\} \rangle. \quad (9)$$

$f_L(\omega)$ [$f_R(\omega)$] is the Fermi distribution function in lead L [R]. The level broadening is renormalized as $\tilde{\Gamma} = \Gamma/(1 + \xi)$. $\alpha = 4\Gamma_L\Gamma_R/\Gamma^2$ is the asymmetric factor of the quantum dot.

We consider the tunnel couplings in H_T exactly before taking the e-ph interaction into account. In the absence of the interaction, the retarded Green function is given by the equation-of-motion method [see Appendix A],

$$G_{\text{dd}}^{r(0)}(\omega) = \frac{1}{\omega - \varepsilon_0 + \frac{1}{4}\sqrt{\alpha T_r}\Gamma \cos \varphi + \frac{i}{2}\tilde{\Gamma}}. \quad (10)$$

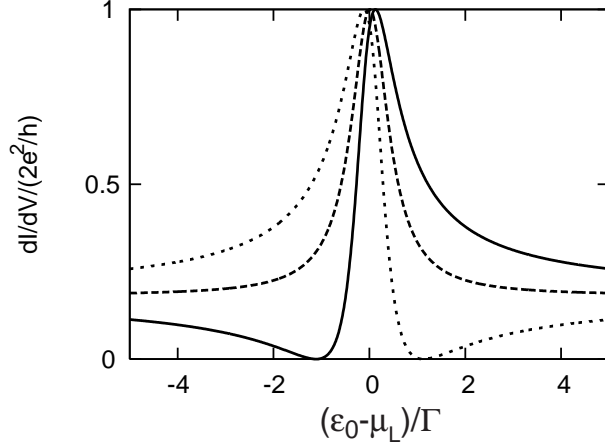


FIG. 2: The differential conductance as a function of the dot level ε_0 in the absence of e-ph interaction. The phase by the magnetic flux inside the ring is $\varphi = 0$ (dotted line), $\varphi = \pi/2$ (dashed line), and $\varphi = \pi$ (solid line). We fix $\xi = \pi^2 \nu^2 W^2 = 0.05$ ($T_r = 0.18$) and asymmetric factor $\alpha = 1$.

The differential conductance dI/dV at zero temperature is expressed as

$$dI/dV = \frac{2e^2}{h} T_r \frac{|\tilde{\varepsilon} + q_F \tilde{\Gamma}/2|^2}{\tilde{\varepsilon}^2 + \tilde{\Gamma}^2/4}, \quad (11)$$

where $\tilde{\varepsilon} = \mu_L - \varepsilon_0 + \frac{1}{4}\sqrt{\alpha T_r} \Gamma \cos \varphi$.¹³ This is an extended Fano form⁵ with a complex parameter q_F ,

$$q_F = \sqrt{\frac{\alpha}{T_r}} (\sqrt{1 - T_r} \cos \varphi + i \sin \varphi). \quad (12)$$

Figure 2 shows the differential conductance as a function of the dot level ε_0 , with $\alpha = 1$ and $\xi = 0.05$ ($T_r = 0.18$). We observe a Fano resonance with dip and peak when $\varphi = 0$. With increasing φ , the asymmetric resonant-shape changes to symmetric ($\varphi = \pi/2$), and to asymmetric with peak and dip ($\varphi = \pi$). This is in agreement with the experimental results.³

III. TREATMENT OF E-PH INTERACTION

We consider the e-ph interaction by the perturbation expansion; second-order perturbation in the case of optical phonons and self-consistent Born approximation in the case of acoustic phonons.^{17,18} For the comparison, we also examine the Breit-Wigner resonance with optical phonons by the canonical transformation method.^{20,23}

A. Keldysh Green function

To examine the current under a finite bias, we use the Keldysh Green function formalism. The Green function of the quantum dot is defined by

$$\mathbf{G}_{\text{dd}}(\omega) = \begin{pmatrix} G_{\text{dd}}^t(\omega) & -G_{\text{dd}}^<(\omega) \\ G_{\text{dd}}^>(\omega) & -G_{\text{dd}}^{\tilde{t}}(\omega) \end{pmatrix}, \quad (13)$$

where the elements are the Fourier transforms of

$$G_{\text{dd}}^t(t-t') = -i\mathcal{T}\langle d(t)d^\dagger(t') \rangle, \quad (14)$$

$$G_{\text{dd}}^{\tilde{t}}(t-t') = -i\tilde{\mathcal{T}}\langle d(t)d^\dagger(t') \rangle, \quad (15)$$

$$G_{\text{dd}}^<(t-t') = i\langle d^\dagger(t')d(t) \rangle, \quad (16)$$

$$G_{\text{dd}}^>(t-t') = -i\langle d(t)d^\dagger(t') \rangle, \quad (17)$$

respectively. The unperturbed Green function, $\mathbf{G}_{\text{dd}}^{(0)}(\omega)$, is defined in the same way. They satisfy the Dyson equation²⁸

$$\mathbf{G}_{\text{dd}}(\omega) = \mathbf{G}_{\text{dd}}^{(0)}(\omega) + \mathbf{G}_{\text{dd}}^{(0)}(\omega)\mathbf{\Sigma}(\omega)\mathbf{G}_{\text{dd}}(\omega), \quad (18)$$

where $\mathbf{\Sigma}(\omega)$ is the self-energy by the e-ph interaction

$$\mathbf{\Sigma}(\omega) = \begin{pmatrix} \Sigma^t(\omega) & -\Sigma^<(\omega) \\ \Sigma^>(\omega) & -\Sigma^{\tilde{t}}(\omega) \end{pmatrix}. \quad (19)$$

We need the retarded Green function $G_{\text{dd}}^r(\omega)$ in Eq. (8) to obtain the transport properties. It is expressed as

$$G_{\text{dd}}^r(\omega) = G_{\text{dd}}^t(\omega) - G_{\text{dd}}^<(\omega). \quad (20)$$

$G_{\text{dd}}^r(\omega)$ follows the Dyson equation of

$$G_{\text{dd}}^r(\omega) = G_{\text{dd}}^{r(0)}(\omega) + G_{\text{dd}}^{r(0)}(\omega)\Sigma^r(\omega)G_{\text{dd}}^r(\omega), \quad (21)$$

where the self-energy is given by

$$\Sigma^r(\omega) = \Sigma^t(\omega) - \Sigma^<(\omega). \quad (22)$$

Since $G_{\text{dd}}^{r(0)}(\omega)$ is given by Eq. (10), Eq. (21) yields the expression of

$$G_{\text{dd}}^r(\omega) = \frac{1}{\omega - \varepsilon_0 + \frac{1}{4}\sqrt{\alpha T_r}\Gamma \cos \varphi + \frac{1}{2}i\tilde{\Gamma} - \Sigma^r(\omega)}. \quad (23)$$

By calculating $\Sigma^t(\omega)$ and $\Sigma^<(\omega)$, we obtain $\Sigma^r(\omega)$ by Eq. (22) and hence $G_{\text{dd}}^r(\omega)$ by Eq. (23).

B. Perturbation expansion

In the second-order perturbation of e-ph interaction, the elements of the self-energy, Eq. (19), are written as

$$\Sigma^\gamma(\omega) = \frac{i}{2\pi} \sum_{\mathbf{q}} |M_{\mathbf{q}}|^2 \int d\omega' G_{\text{dd}}^{\gamma(0)}(\omega - \omega') D^\gamma(\mathbf{q}, \omega') \quad (24)$$

(γ stands for $t, t', <, >$). To obtain $\Sigma^t(\omega)$ and $\Sigma^<(\omega)$, we need $G_{\text{dd}}^{t(0)}(\omega)$, $G_{\text{dd}}^{<(0)}(\omega)$ and Green functions of phonon, $D^t(\mathbf{q}, \omega)$, $D^<(\mathbf{q}, \omega)$.

$G_{\text{dd}}^{<(0)}(\omega)$ is calculated using the equation-of-motion method [see Appendix A] as

$$\begin{aligned} G_{\text{dd}}^{<(0)}(\omega) = & G_{\text{dd}}^{r(0)}(\omega) \left\{ \frac{i}{2} \tilde{\Gamma} \sqrt{\alpha T_r} \sin \varphi [f_L(\omega) - f_R(\omega)] \right. \\ & \left. + \frac{i}{(1 + \xi)^2} [(\Gamma_L + \xi \Gamma_R) f_L(\omega) + (\Gamma_R + \xi \Gamma_L) f_R(\omega)] \right\} G_{\text{dd}}^{a(0)}(\omega), \end{aligned} \quad (25)$$

where $G_{\text{dd}}^{r(0)}(\omega)$ is given by Eq. (10) and $G_{\text{dd}}^{a(0)}(\omega) = [G_{\text{dd}}^{r(0)}(\omega)]^*$. $G_{\text{dd}}^{t(0)}(\omega)$ is given by the relation, $G_{\text{dd}}^{t(0)}(\omega) = G_{\text{dd}}^{r(0)}(\omega) + G_{\text{dd}}^{<(0)}(\omega)$.

The Fourier transforms of phonon Green functions are

$$\begin{aligned} D^t(\mathbf{q}, \omega) = & -2\pi i [N_{\mathbf{q}} \delta(\omega + \omega_{\mathbf{q}}) + N_{\mathbf{q}} \delta(\omega - \omega_{\mathbf{q}})] \\ & + \frac{1}{\omega - \omega_{\mathbf{q}} + i\delta} - \frac{1}{\omega + \omega_{\mathbf{q}} - i\delta}, \end{aligned} \quad (26)$$

$$\begin{aligned} D^<(\mathbf{q}, \omega) = & -2\pi i [(N_{\mathbf{q}} + 1) \delta(\omega + \omega_{\mathbf{q}}) \\ & + N_{\mathbf{q}} \delta(\omega - \omega_{\mathbf{q}})]. \end{aligned} \quad (27)$$

$N_{\mathbf{q}}$ denotes the phonon occupation number, $1/[\exp(\omega_{\mathbf{q}}/k_B T) - 1]$. We fix the temperature at $T = 0$ in the calculations.

For the self-consistent Born approximation, $G_{\text{dd}}^{\gamma(0)}(\omega - \omega')$ in Eq. (24) is replaced by $G_{\text{dd}}^\gamma(\omega - \omega')$ as

$$\Sigma^t(\omega) = \frac{i}{2\pi} \sum_{\mathbf{q}} |M_{\mathbf{q}}|^2 \int d\omega' G_{\text{dd}}^t(\omega - \omega') D^t(\mathbf{q}, \omega'), \quad (28)$$

and

$$\Sigma^<(\omega) = \frac{i}{2\pi} \sum_{\mathbf{q}} |M_{\mathbf{q}}|^2 \int d\omega' G_{\text{dd}}^{<}(\omega - \omega') D^<(\mathbf{q}, \omega'). \quad (29)$$

From the Dyson equation, Eq. (18), $G_{\text{dd}}^{<}(\omega)$ is expressed as

$$G_{\text{dd}}^{<}(\omega) = [1 + G_{\text{dd}}^r(\omega) \Sigma^r(\omega)] G_{\text{dd}}^{<(0)}(\omega) [1 + \Sigma^a(\omega) G_{\text{dd}}^a(\omega)] + G_{\text{dd}}^r(\omega) \Sigma^<(\omega) G_{\text{dd}}^a(\omega). \quad (30)$$

The substitution of Eqs. (23) and (25) into Eq. (30) yields

$$G_{\text{dd}}^<(\omega) = \frac{1}{[\omega - \varepsilon_0 + \frac{1}{4}\sqrt{\alpha T_r}\Gamma \cos \varphi - \text{Re}\Sigma^r(\omega)]^2 + [\frac{1}{2}\tilde{\Gamma} - \text{Im}\Sigma^r(\omega)]^2} \times \left\{ \frac{i}{2}\tilde{\Gamma}\sqrt{\alpha T_r} \sin \varphi [f_L(\omega) - f_R(\omega)] + \frac{i}{(1 + \xi)^2} [(\Gamma_L + \xi\Gamma_R)f_L(\omega) + (\Gamma_R + \xi\Gamma_L)f_R(\omega)] + \Sigma^<(\omega) \right\}. \quad (31)$$

$G_{\text{dd}}^t(\omega)$ is obtained by Eq. (20), using $G_{\text{dd}}^<(\omega)$ in Eq. (31) and $G_{\text{dd}}^r(\omega)$ in Eq. (23). We determine $\Sigma^r(\omega)$ and $\Sigma^<(\omega)$ by solving the equations self-consistently.

C. Canonical transformation

For the comparison with the perturbative method, we examine the canonical transformation method.^{20,23} In this method, we decouple the e-ph interaction in Eq. (5) by a canonical transformation of²⁸

$$\bar{H} = e^s H e^{-s}, \quad (32)$$

$$s = d^\dagger d \sum_{\mathbf{q}} \frac{M_{\mathbf{q}}}{\omega_{\mathbf{q}}} (a_{-\mathbf{q}}^\dagger - a_{\mathbf{q}}). \quad (33)$$

By the transformation, the Hamiltonians for electrons in the quantum dot, e-ph interaction, and phonons are rewritten as

$$\bar{H}_D + \bar{H}_{\text{e-ph}} + \bar{H}_{\text{ph}} = [\varepsilon_0 - \sum_{\mathbf{q}} (M_{\mathbf{q}}^2/\omega_{\mathbf{q}})] d^\dagger d + \sum_{\mathbf{q}} \omega_{\mathbf{q}} a_{\mathbf{q}}^\dagger a_{\mathbf{q}}. \quad (34)$$

The tunneling Hamiltonian, Eq. (4), is transformed to

$$\begin{aligned} \bar{H}_T = & \sum_k (t_L c_{Lk}^\dagger \bar{d} + \text{H.c.}) \\ & + \sum_k (t_R c_{Rk}^\dagger \bar{d} + \text{H.c.}) \\ & + \sum_{k,k'} (W e^{i\varphi} c_{Rk'}^\dagger c_{Lk} + \text{H.c.}), \end{aligned} \quad (35)$$

where \bar{d} and \bar{d}^\dagger are renormalized operators of electrons,

$$\bar{d} = e^s d e^{-s} = dX, \quad (36)$$

$$\bar{d}^\dagger = e^s d^\dagger e^{-s} = d^\dagger X^\dagger \quad (37)$$

with

$$X = \exp \left[- \sum_{\mathbf{q}} \frac{M_{\mathbf{q}}}{\omega_{\mathbf{q}}} (a_{\mathbf{q}}^\dagger - a_{\mathbf{q}}) \right]. \quad (38)$$

After the decoupling of electron and phonon operators in Eq. (34), we take into account the e-ph interaction exactly, whereas we adopt an approximation for \bar{H}_T : Electron operators, \bar{d} and \bar{d}^\dagger , are replaced by d and d^\dagger , disregarding the e-ph interaction in the tunnel couplings. The retraded Green function $G_{\text{dd}}^r(t - t')$ is given in Appendix C.

IV. OPTICAL PHONONS

We begin with the case of longitudinal optical phonons. To illustrate the decoherence—zero-point fluctuation effect in the elastic process and dephasing effect in the inelastic process—, we mainly discuss the effects on the Breit-Wigner resonance in this section.

The amplitude of the e-ph interaction is described by the Fröhlich-coupling²⁸

$$\lambda_{\mathbf{q}} = i \frac{1}{\sqrt{V}} \sqrt{4\nu_{\text{e-ph}}} \frac{\omega_{\mathbf{q}}}{|\mathbf{q}|} \left(\frac{1}{2m^*\omega_{\mathbf{q}}} \right)^{1/4}, \quad (39)$$

$$\nu_{\text{e-ph}} = e^2 \sqrt{\frac{m^*}{2\omega_{\mathbf{q}}}} \left[\frac{1}{\varepsilon(\infty)} - \frac{1}{\varepsilon(0)} \right], \quad (40)$$

where m^* is the effective mass of electrons. $\varepsilon(\infty)$ and $\varepsilon(0)$ are the dielectric constants at high and low frequencies, respectively. V is the normalization volume. As a good approximation, we assume that all the phonons have the same energy ω_0 (Einstein model) since the wavenumbers are limited to a small range of $|\mathbf{q}| \lesssim 2\pi/L$, when L is in the submicron scale. We define the coupling strength of the e-ph interaction as

$$\zeta^2 = \sum_{\mathbf{q}} M_{\mathbf{q}}^2. \quad (41)$$

A. Breit-Wigner resonance

We examine the Breit-Wigner resonance through a quantum dot without the reference arm ($\xi = 0$, $T_r = 0$). We treat the e-ph interaction by the second-order perturbation. In Fig. 3, we plot the differential conductance, dI/dV , as a function of the energy level ε_0 in the

quantum dot. The bias-voltage is $eV = 0.5\Gamma$ ($eV < \omega_0 = 2\Gamma$; dashed line) and 3Γ ($eV > \omega_0$; solid line). A dotted line indicates the conductance in the absence of the e-ph interaction, where the conductance is independent of the bias. A subpeak at $\varepsilon_0 - \mu_L \approx -\omega_0$ is seen only when $eV > \omega_0$, which corresponds to the emission of a phonon.

When $eV < \omega_0$, a real process of phonon emission cannot take place at $T = 0$. Even in this case, the peak height is suppressed by the e-ph interaction. This is due to the elastic process in which electrons emit and absorb phonons virtually. It disturbs the coherent transport through the quantum dot and hence diminishes the resonant peak height. When $eV > \omega_0$, both elastic and inelastic processes are possible. The latter process makes the subpeak of the phonon emission, whereas the former process mainly suppresses the main peak, as discussed in the next section.

The position of the main peak is shifted by the e-ph interaction, regardless of $eV < \omega_0$ or $eV > \omega_0$. This is ascribable to the above-mentioned elastic process. The zero-point fluctuation of phonons results in the renormalization of the energy level in the quantum dot, in addition to the suppression of the peak height.

The width of the main peak is influenced by the inelastic process of phonon emission: it does not change when $eV < \omega_0$, whereas it is broadened when $eV > \omega_0$ although it is not clearly seen in Fig. 3. To discuss the width, we examine the retarded Green function in Eq. (23). The peak width is determined by the imaginary part of the self-energy $\Sigma^r(\omega)$ in its denominator. When $eV < \omega_0$, $\text{Im}\Sigma^r(\omega) = 0$ in the range of integration, $0 \leq \omega \leq eV$, in Eq. (8). Hence the peak width is not changed. We conclude that the peak width is not influenced by the elastic process of virtual emission and absorption of phonons in the resonant tunneling. This is in contrast to the sequential tunneling where the renormalization of the phonon state reduces the effective tunnel coupling between the quantum dot and leads.²⁴ When $eV > \omega_0$, on the other hand, $\text{Im}\Sigma^r(\omega) \neq 0$. At $\omega = eV$,

$$\text{Im}\Sigma^r(eV) = -\frac{\zeta^2}{4} \frac{\Gamma}{(eV - \omega_0 - \varepsilon_0)^2 + \Gamma^2/4}, \quad (42)$$

which mainly determines the linewidth of the differential conductance. Since $\text{Im}\Sigma^r(eV) < 0$, the linewidth is broadened by the e-ph interaction. The real emission of phonons decreases the life-time of the dot state and, as a result, increases the peak width.

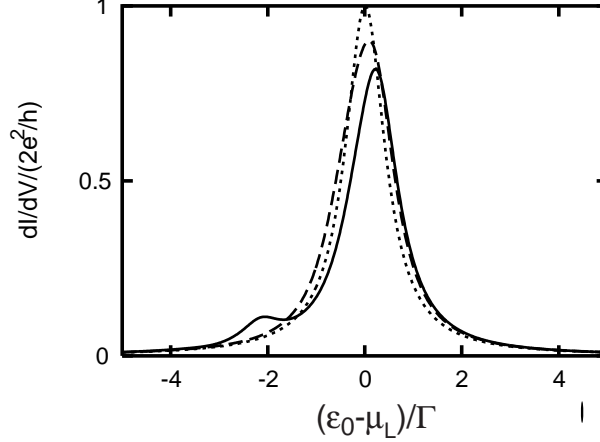


FIG. 3: The differential conductance as a function of the dot level ε_0 , in the case of Breit-Wigner resonance ($\xi = 0$, $T_r = 0$) with optical phonons. The asymmetric factor is $\alpha = 1$. The phonon energy is $\omega_0 = 2\Gamma$, whereas the strength of e-ph coupling is $\zeta = 0.8\Gamma$. The bias voltage is $eV = 0.5\Gamma$ (dashed line) and 3Γ (solid line). Dotted line indicates the conductance in the absence of e-ph interaction.

B. Elastic and inelastic processes

To investigate the elastic and the inelastic processes more precisely, we perform the calculation considering the elastic process only. Among the four elements in the self-energy $\Sigma(\omega)$, Eq. (19), the diagonal elements, Σ^t and $\Sigma^{\bar{t}}$, describe the elastic process while the off-diagonal elements, $\Sigma^<$ and $\Sigma^>$, represent the inelastic process, as discussed in Appendix B. Excluding the latter, the retarded Green function is written as

$$G_{\text{dd}}^r(\omega) = G_{\text{dd}}^{r(0)}(\omega) + G_{\text{dd}}^{t(0)}(\omega)\Sigma^t(\omega)G_{\text{dd}}^r(\omega) + G_{\text{dd}}^{<(0)}(\omega)\Sigma^{\bar{t}}(\omega)G_{\text{dd}}^r(\omega). \quad (43)$$

In Fig. 4, we present the calculated results using Eq. (43) by dashed lines. Solid lines indicate the results in the presence of both elastic and inelastic processes. When $eV < \omega_0$ [Fig. 4(a)], both the results are identical to each other since only the elastic process exists. When $eV > \omega_0$ [Fig. 4(b)], the inelastic process makes some differences. The height of the dashed line and solid line are almost the same, which indicates that the suppression of the main peak is mostly caused by the elastic process. Note that the elastic process also results in a subpeak at $\varepsilon_0 - \mu_L \approx -\omega_0$ when $eV > \omega_0$. This is due to the formation of so-called

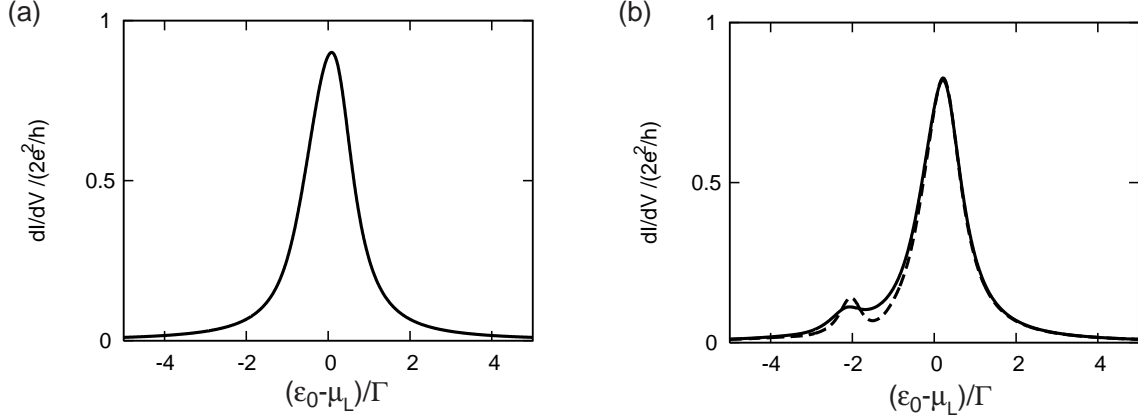


FIG. 4: Differential conductance as a function of the dot level ε_0 in the case of Breit-Wigner resonance ($\xi = 0$, $T_r = 0$) with optical phonons. The asymmetric factor is $\alpha = 1$. The phonon energy is $\omega_0 = 2\Gamma$, whereas the strength of e-ph coupling is $\zeta = 0.8\Gamma$. The bias voltage is (a) $eV = 0.5\Gamma$ and (b) 3Γ . The dashed line includes only the elastic process of e-ph interaction. The solid line includes both the elastic and inelastic processes. Note that dashed and solid lines are overlapped by each other in (a).

polaron in which an electron is coherently coupled with phonons. The resonant tunneling through a polaron level makes the subpeak. The polaron has a finite lifetime by the real emission of phonon. Hence the inelastic process broadens the subpeak as well as the main peak.

C. Fano resonance

Figure 5 shows the Fano resonance with optical phonons, in the presence of reference arm ($x = 0.05$, $T_r = 0.18$). The magnetic phase is (a) $\varphi = 0$, (b) $\varphi = \pi/2$, and (c) $\varphi = \pi$. The differential conductance, dI/dV , is plotted as a function of the energy level ε_0 in the quantum dot, when $eV < \omega_0$ (dashed line) or $eV > \omega_0$ (solid line). The dotted line indicates the non-interacting case.

The influence of the e-ph interaction on the Fano resonance is qualitatively the same as that on the Breit-Wigner resonance. When $eV < \omega_0$, only the elastic process takes place. Then we do not observe a subpeak of phonon emission. The zero-point fluctuation of phonons reduces the resonant amplitude; both the resonant peak and dip are diminished.

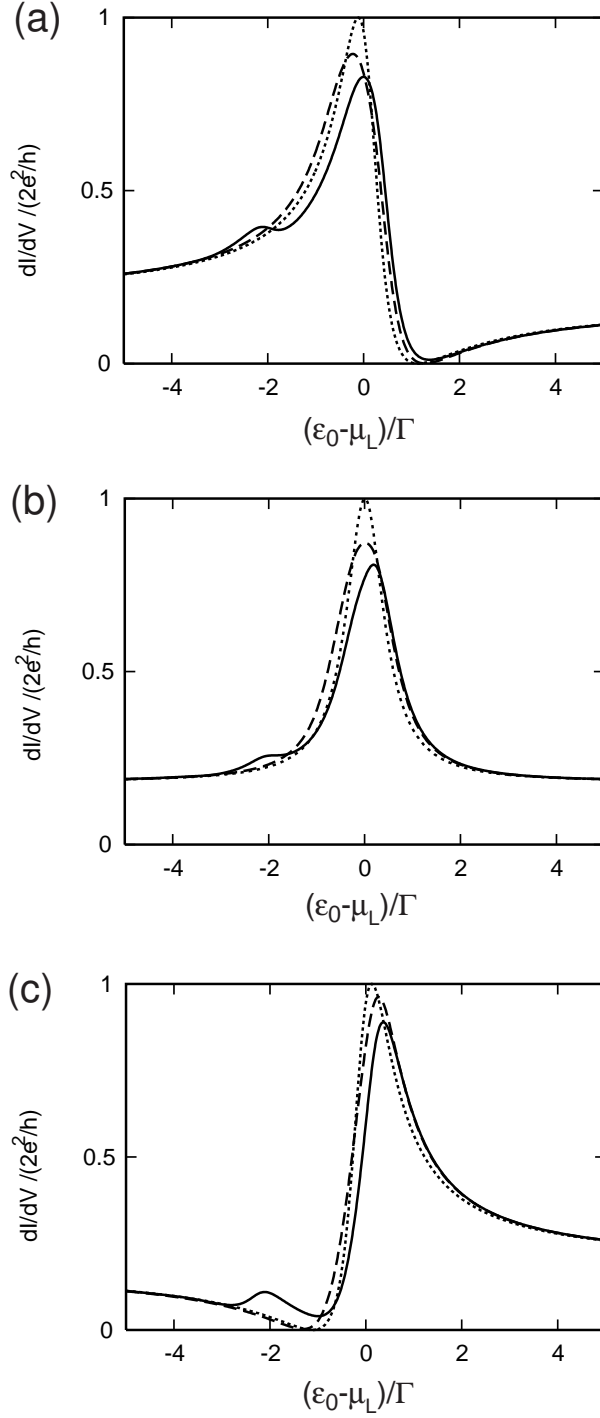


FIG. 5: Differential conductance as a function of the dot level ε_0 in the Fano resonance ($\xi = 0.05$, $T_r = 0.18$). The asymmetric factor is $\alpha = 1$. The phonon energy is $\omega_0 = 2\Gamma$, whereas the strength of e-ph coupling is $\zeta = 0.8\Gamma$. The magnetic phase is (a) $\varphi = 0$, (b) $\varphi = \pi/2$, and (c) $\varphi = \pi$. The bias voltage is $eV = 0.5\Gamma$ (dashed lines) and 3Γ (solid lines). The dotted lines indicate the case in the absence of e-ph interaction.

The resonant width is not changed by the elastic process. When $eV > \omega_0$, a subpeak appears by the real emission of phonon. The inelastic process broadens the width of main resonance.

The shape of the Fano resonance changes with magnetic phase φ in the same way as in Fig. 2. We find that the renormalization of the phase is negligibly small.

D. Calculation by canonical transformation method

In this subsection, we consider the e-ph interaction by the canonical transformation method. By the method, the retarded Green function is easily obtained as^{23,28}

$$G_{\text{dd}}^r(\omega) = e^{-k(2N_{\mathbf{q}}+1)} \sum_{l=-\infty}^{\infty} J_l[2k\sqrt{N_{\mathbf{q}}(N_{\mathbf{q}}+1)}] \times \frac{e^{l\omega_0\beta/2}}{\omega - (\varepsilon_0 - \Delta) - l\omega_0 + \frac{1}{4}\sqrt{\alpha T_r}\Gamma \cos \varphi + \frac{i}{2}\tilde{\Gamma}}, \quad (44)$$

where $J_l(x)$ are the Bessel functions. $k = (\zeta/\omega_0)^2$ and energy shift is $\Delta = \zeta^2/\omega_0$. At zero temperature, $G_{\text{dd}}^r(\omega)$ is expressed as

$$G_{\text{dd}}^r(\omega) = e^{-k} \sum_{l=-\infty}^0 \frac{k^l/l!}{\omega - (\varepsilon_0 - \Delta) - l\omega_0 + \frac{1}{4}\sqrt{\alpha T_r}\Gamma \cos \varphi + \frac{i}{2}\tilde{\Gamma}}. \quad (45)$$

The substitution of Eq. (45) into Eq. (8) yields the differential conductance. In the case of Breit-Wigner resonance ($\xi = 0$, $T_r = 0$),

$$dI/dV = \frac{2e^2}{h} \sum_{l=-\infty}^0 \frac{\Gamma^2}{4} \frac{e^{-k} k^l/l!}{[\mu_L - (\varepsilon_0 - \Delta) - l\omega_0]^2 + \Gamma^2/4}. \quad (46)$$

In the case of Fano resonance,

$$dI/dV = \frac{2e^2}{h} e^{-k} T_r \sum_{l=-\infty}^0 \frac{k^l}{l!} \frac{|\tilde{\varepsilon}_l + q_F \tilde{\Gamma}/2|^2}{\tilde{\varepsilon}_l^2 + \tilde{\Gamma}^2/4}, \quad (47)$$

where $\tilde{\varepsilon} = \mu_L - (\varepsilon_0 - \Delta) - l\omega_0 + \frac{1}{4}\sqrt{\alpha T_r}\Gamma \cos \varphi$.

The calculated results are shown in Fig. 6, (a) Breit-Wigner resonance and (b) Fano resonance. In the case of Breit-Wigner resonance, the main peak ($l = 0$) is given by the Lorentzian form with center at $\varepsilon_0 - \mu_L = \Delta$, indicating the renormalization of the energy level. The peak height is reduced by the factor of e^{-k} , whereas the width is fixed at $\Gamma/2$. A subpeak is seen at $\varepsilon_0 - \mu_L = \Delta - \omega_0$, corresponding to the emission of a phonon. Hence the polaron formation can be described by this calculation method, similarly to the Tien-Gordon

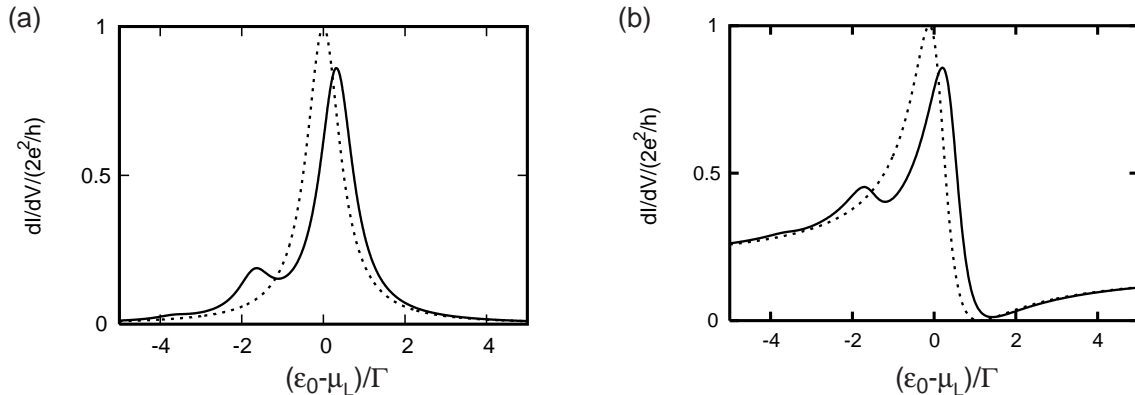


FIG. 6: Differential conductance as a function of the dot level ϵ_0 with optical phonons, calculated by the canonical transformation method. The asymmetric factor is $\alpha = 1$. The phonon energy is $\omega_0 = 2\Gamma$, whereas the strength of e-ph coupling is $\zeta = 0.8\Gamma$. Dotted line indicates the differential conductance in the absence of e-ph interaction. (a) Case of resonant tunneling through a quantum dot ($\xi = 0$, $T_r = 0$). (b) The case of Fano resonance ($\xi = 0.05$, $T_r = 0.18$).

theory.³⁰ The calculated results of Fano resonance can be understood in the same way as those of the Breit-Wigner resonance.

We find some shortcomings of this method. (i) The bias-voltage dependence of the transport cannot be obtained. The dI/dV curve is independent of the bias in Eqs. (46) and (47). Hence the inelastic process of phonon emission takes place even when $eV < \omega_0$. The renormalization of the energy level by the e-ph interaction does not depend on the bias voltage. (ii) The resonant width of the main peak is not changed by the phonon emission. Hence the finite lifetime by the inelastic process is not considered properly. These are due to the approximation in the tunnel Hamiltonian. By the replacement of the electron operator \bar{d} by d in \bar{H}_T [Eq. (35)], we neglect the change of the phonon states accompanied by the tunnel processes.

V. ACOUSTIC PHONONS

Now we discuss the e-ph interaction with acoustic phonons. The amplitude of the e-ph interaction in Eq. (7) is described by the piezoelectric coupling,^{22,31}

$$|\lambda_{\mathbf{q}}|^2 = g \frac{\pi^2 c_s^2}{V|\mathbf{q}|}, \quad (48)$$

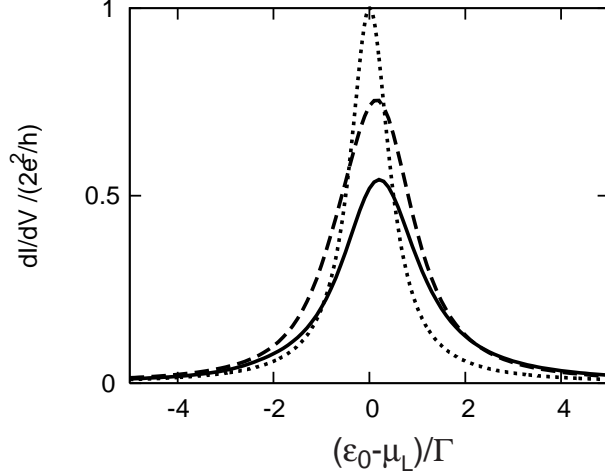


FIG. 7: Differential conductance as a function of the dot level ε_0 in the Breit-Wigner resonance with acoustic phonons. The asymmetric factor is $\alpha = 1$. The coupling constant is $g = 0.05$, whereas the dot size is $L = c_s/(2\Gamma)$. The bias voltage is $eV = 0.5\Gamma$ (dashed line) and 2Γ (solid line). The dotted line indicates the conductance in the absence of e-ph interaction.

where g is a coupling constant and c_s is the sound velocity. The dispersion relation of the phonons is given by

$$\omega_{\mathbf{q}} = c_s |\mathbf{q}|. \quad (49)$$

For the convenience of the calculation, we assume that $|\langle d|e^{i\mathbf{q}\cdot\mathbf{r}}|d\rangle|^2$ is given by

$$|\langle d|e^{i\mathbf{q}\cdot\mathbf{r}}|d\rangle|^2 = \frac{\sqrt{2}}{\pi^{1/2}L^2} \frac{1}{q^2 + (1/L)^2} \quad (50)$$

in Eq. (7). For the calculation of e-ph interaction, we adopt the self-consistent Born approximation.

A. Breit-Wigner resonance

We begin with the Breit-Wigner resonance in the absence of reference arm ($\xi = 0$, $T_r = 0$). We set $g = 0.05$ and $c_s = 5000\text{m/s}$, which are the values in GaAs.^{19,31} We fix $L = c_s/(2\Gamma)$: e. g. when $\Gamma = 0.1\text{meV}$, the dot size is $L = 0.015\mu\text{m}$ (smaller than in Ref. [3]). The differential conductance is plotted in Fig. 7, as a function of the energy level ε_0 in the quantum dot. The bias voltage is $eV = 0.5\Gamma$ (dashed line) and 2Γ (solid line). In contrast to the case of optical phonons (Sec. IV), the inelastic process always exists, which is accompanied by the

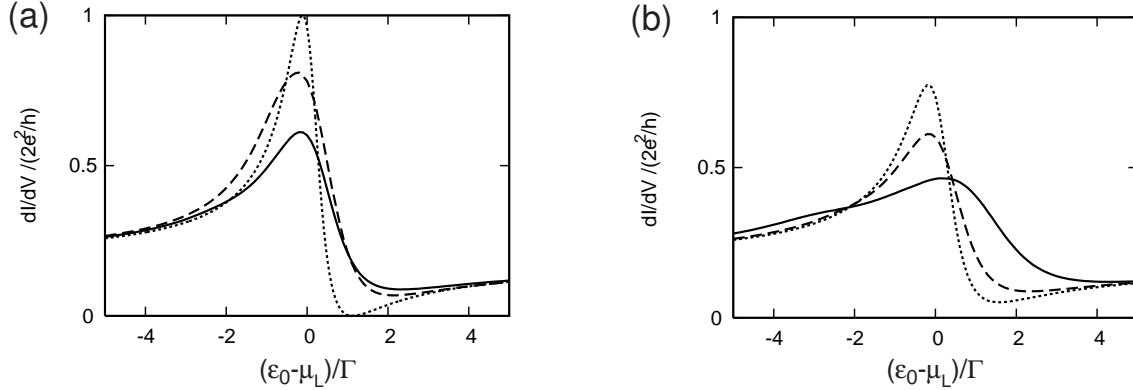


FIG. 8: Differential conductance as a function of the dot level ϵ_0 in the Fano resonance with acoustic phonons. We set $\xi = 0.05$ ($T_r = 0.18$). The asymmetric factor is $\alpha = 1$. The coupling constant is $g = 0.05$. (a) The dot size is fixed at $L = c_s/(2\Gamma)$. The bias voltage is $eV = 0.5\Gamma$ (dashed line) and 2Γ (solid line). The dotted line indicates the conductance in the absence of e-ph interaction. (b) We change the dot size as $L = c_s/\Gamma$ (dotted line), $c_s/(2\Gamma)$ (dashed line), and $c_s/(5\Gamma)$ (solid line). The bias voltage is $eV = 2\Gamma$.

real emission of phonons. A subpeak structure is not observed since the acoustic phonon has a continuous spectrum.

We find the following effects of the e-ph interaction. (i) The resonant peak height decreases with increasing the bias voltage. As discussed in the previous section, this should be mainly ascribable to the elastic process. (ii) The peak width is more broadened with the bias voltage, which is due to the inelastic process. The emission of phonons results in the finite lifetime and hence an increase in the resonant width. (iii) The form of the Breit-Wigner resonance becomes asymmetric. The resonant peak is more suppressed on the side of $\epsilon_0 < \mu_L$ than on the side of $\epsilon_0 > \mu_L$. This may be explained as follows. When $\epsilon_0 < \mu_L$, phonons can be emitted in the electron tunneling from lead L to the quantum dot, or in the tunneling from the dot to lead R. When $\epsilon_0 > \mu_L$, phonons can be emitted only in the latter. Hence the decoherence works differently on both sides of the resonance.

B. Fano resonance

Figure 8(a) shows the Fano resonance with acoustic phonons, in the presence of reference arm ($\xi = 0.05$, $T_r = 0.18$). The bias voltage is $eV = 0.5\Gamma$ (dashed line) and 2Γ (solid line).

A subpeak structure is not seen as in the Breit-Wigner resonance with acoustic phonons.

The e-ph interaction decreases the resonant amplitude, whereas it increases the resonant width, reflecting the real emission of phonons. These effects are more prominent with larger bias. Particularly, the resonant dip becomes almost invisible with high bias and as a result, the asymmetric shape of the Fano resonance grows like a symmetric one. Although this is in qualitative accordance with the experimental results,³ the resonant peak is still in an asymmetric form even in a smaller size of quantum dots (with stronger e-ph interaction, as discussed below) than in the experiment. To explain the experimental results quantitatively, we would have to consider the e-ph interaction in the reference arm as well as inside the quantum dot. The other dephasing effects, e.g. spin-flip of a localized electron in the quantum dot, might be also important.

We change the size of the quantum dot, L , in Fig. 8(b): $L = c_s/\Gamma$ (dotted line), $c_s/(2\Gamma)$ (dashed line), and $c_s/(5\Gamma)$ (solid line). The bias voltage is fixed at $eV = 2\Gamma$. With an decrease in the dot size, the matrix element $\langle d|e^{i\mathbf{q}\cdot\mathbf{r}}|d\rangle$ in the coupling coefficient $M_{\mathbf{q}}$ increases [see Eq. (50)]. In consequence, the effect of e-ph interaction is enhanced. The figure indicates smaller amplitudes and wider widths of the resonance in smaller quantum dots.

VI. CONCLUSIONS

We have investigated the Breit-Wigner resonance and Fano resonance in quantum dots with e-ph interaction. Using Keldysh Green function method and perturbation with respect to the e-ph interaction, we have obtained the bias-voltage (V) dependence of the decoherence.

With optical phonons of energy ω_0 , we distinguish elastic and inelastic processes. When $eV < \omega_0$, only the elastic process takes place in which electrons emit and absorb phonons virtually. The process suppresses the resonant amplitude, whereas it does not change the resonant width. We do not observe the renormalization of the tunnel coupling which has been discussed in the sequential tunneling.²⁴ When $eV > \omega_0$, the inelastic process is possible, which broadens the resonant width. The process also makes a subpeak, as a function of the energy level in the quantum dot, corresponding to the real emission of phonons. We cannot obtain any bias-voltage dependence of the decoherence when we consider the e-ph interaction by the canonical transformation method, neglecting its effect on the tunnel coupling.

With acoustic phonons, the suppression of resonant amplitude and broadening of the

resonant width are more prominent with an increase in the bias. In the Fano resonance, the resonant dip becomes almost invisible. The asymmetric resonant shape becomes like a symmetric one, in qualitative accordance with the experimental results.³ However, the model with e-ph interaction in the quantum dot only is not sufficient for the quantitative explanation of the experiment.

In the present paper, we use the term of dephasing for the real emission of phonons in the inelastic process. This is because the elastic process does not result in the dephasing, as discussed in Ref. 24. In the presence of reference arm, one might think that the dephasing effect can be directly evaluated by calculating the amplitude of AB oscillation. But it is not correct. The e-ph interaction leads to the elastic and inelastic processes in the quantum dot on one hand, it changes the ratio of the current through the reference arm to that through the quantum dot on the other hand. Hence the amplitude of the AB oscillation cannot measure the dephasing effect correctly.

The authors gratefully acknowledge discussions with F. Marquardt. This work was partially supported by a Grant-in-Aid for Scientific Research in Priority Areas ‘‘Semiconductor Nanospintronics’’ (No. 14076216) of the Ministry of Education, Culture, Sports, Science and Technology, Japan.

APPENDIX A: EXPRESSION OF CURRENT

The current from lead L to the quantum dot is given by the time derivative of the occupation number in lead L,

$$I_L = -e\langle \dot{N}_L \rangle = -ie\langle [H, N_L] \rangle, \quad (\text{A1})$$

with $N_L = \sum_k c_{Lk}^\dagger c_{Lk}$. A straightforward calculation yields

$$\begin{aligned} I_L &= ie \left\{ \sum_k [t_L \langle c_{Lk}^\dagger d \rangle - t_L \langle d^\dagger c_{Lk} \rangle] + \sum_{k,k'} [W e^{-i\varphi} \langle c_{Lk}^\dagger c_{Rk'} \rangle - W e^{i\varphi} \langle c_{Rk'}^\dagger c_{Lk} \rangle] \right\} \\ &= 2e \text{Re} \left[t_L \sum_k G_{d,Lk}^<(t, t) + W e^{-i\varphi} \sum_{k,k'} G_{Rk',Lk}^<(t, t) \right]. \end{aligned} \quad (\text{A2})$$

Here, we have introduced lesser Green functions, $G_{d,Lk}^<(t, t') = i\langle c_{Lk}^\dagger(t')d(t) \rangle$ and $G_{Rk',Lk}^<(t, t') = i\langle c_{Lk}^\dagger(t)c_{Rk'}(t') \rangle$. In the energy representation,

$$I_L(\omega) = \frac{2e}{h} \text{Re} \int d\omega [t_L \sum_k G_{d,Lk}^<(\omega) + W e^{-i\varphi} \sum_{k,k'} G_{Rk',Lk}^<(\omega)]. \quad (\text{A3})$$

The current from lead R to the dot, I_R , is obtained in the same way. In the case of non-interaction leads, we can express the current using the Green function of the quantum dot only, as shown in the following.

Let us consider $G_{\text{d,L}k}^<(\omega)$ in Eq. (A3). Using equation-of-motion method and analytic continuation rules,²⁹ $G_{\text{d,L}k}^<(t-t')$ is written as

$$\begin{aligned} G_{\text{d,L}k}^<(t-t') &= \int dt_1 [t_L G_{\text{dd}}^r(t-t_1) g_{\text{L}k}^<(t_1-t') \\ &\quad + t_L G_{\text{dd}}^<(t-t_1) g_{\text{L}k}^a(t_1-t') \\ &\quad + W e^{i\varphi} G_{\text{d,R}k}^r(t-t_1) g_{\text{L}k}^<(t_1-t') \\ &\quad + W e^{i\varphi} G_{\text{d,R}k}^<(t-t_1) g_{\text{L}k}^a(t_1-t')], \end{aligned} \quad (\text{A4})$$

where $G_{\text{d,R}k}^r(t-t') = -i\theta(t-t')\langle\{d(t), c_{\text{R}k}^\dagger(t')\}\rangle$, $G_{\text{d,R}k}^<(t-t') = i\langle c_{\text{R}k}^\dagger(t')d(t)\rangle$, $g_{\text{L}k}^a(t-t') = i\theta(-t+t')\langle\{c_{\text{L}k}(t), c_{\text{L}k}^\dagger(t')\}\rangle$, and $g_{\text{L}k}^<(t-t') = i\langle c_{\text{L}k}^\dagger(t')c_{\text{L}k}(t)\rangle$. The Fourier transformation yields

$$\begin{aligned} \sum_k G_{\text{d,L}k}^<(\omega) &= i\pi\nu t_L G_{\text{dd}}^<(\omega) + 2i\pi\nu f_L(\omega) t_L G_{\text{dd}}^r(\omega) \\ &\quad + i\pi\nu W e^{i\varphi} \sum_k G_{\text{d,R}k}^<(\omega) + 2i\pi\nu f_L(\omega) W e^{i\varphi} \sum_k G_{\text{d,R}k}^r(\omega), \end{aligned} \quad (\text{A5})$$

where $\sum_k g_{\text{L}k}^a(\omega) = i\pi\nu$ and $\sum_k g_{\text{L}k}^<(\omega) = 2i\pi\nu f_L(\omega)$. A similar expression of $\sum_k G_{\text{d,R}k}^<(\omega)$ is obtained in the same way. The expression together with Eq. (A5) yields

$$\begin{aligned} \sum_k G_{\text{d,L(R)}k}^<(\omega) &= \frac{i\pi\nu}{1+\xi} [t_{\text{L(R)}} + i\pi\nu W e^{\pm i\varphi} t_{\text{R(L)}}] G_{\text{dd}}^<(\omega) \\ &\quad + \frac{2i\pi\nu}{1+\xi} [t_{\text{L(R)}} f_{\text{L(R)}}(\omega) + i\pi\nu W e^{\pm i\varphi} t_{\text{R(L)}} f_{\text{R(L)}}(\omega)] G_{\text{dd}}^r(\omega) \\ &\quad + \frac{2i\pi\nu W e^{\pm i\varphi} f_{\text{L(R)}}(\omega)}{1+\xi} \sum_k G_{\text{d,R(L)}k}^r(\omega) \\ &\quad - \frac{2\pi^2\nu^2 W^2 f_{\text{R(L)}}(\omega)}{1+\xi} \sum_k G_{\text{d,L(R)}k}^r(\omega). \end{aligned} \quad (\text{A6})$$

$G_{\text{d,L(R)}k}^r(\omega)$, which appears on the right-hand side of Eq. (A6), is derived from the equation-of-motion method as

$$\begin{aligned} G_{\text{d,L(R)}k}^r(t-t') &= \int dt_1 [t_{\text{L(R)}} G_{\text{dd}}^r(t-t_1) g_{\text{L(R)}k}^r(t_1-t') \\ &\quad + W e^{\pm i\varphi} G_{\text{d,R(L)}k}^r(t-t_1) g_{\text{L(R)}k}^r(t_1-t')], \end{aligned}$$

where $g_{L(R)k}^r(t-t') = -i\theta(t-t')\langle\{c_{L(R)k}(t), c_{L(R)k}^\dagger(t')\}\rangle$. From the Fourier transform, we obtain

$$\sum_k G_{d,L(R)k}^r = \frac{1}{1+\xi}[-i\pi\nu t_{L(R)} - i\pi\nu W e^{\pm i\varphi} t_{R(L)}]G_{dd}^r(\omega). \quad (\text{A7})$$

Then we express $G_{d,L(R)k}^<(\omega)$ in terms of $G_{dd}^r(\omega)$ and $G_{dd}^<(\omega)$.

$G_{Rk',Lk}^<(\omega)$ in Eq. (A3) can be expressed using $G_{dd}^r(\omega)$ and $G_{dd}^<(\omega)$, by the same technique. As a result, the current $I_L(\omega)$ [and also $I_R(\omega)$] is rewritten in terms of $G_{dd}^r(\omega)$ and $G_{dd}^<(\omega)$ only. Finally we delete $G_{dd}^<(\omega)$ by taking a linear combination of them, $I = xI_L - (1-x)I_R$, and obtain Eq. (8).

The expression of unperturbed Green functions, Eqs. (10) and (25), are obtained also by the equation-of-motion method:

$$\begin{aligned} G_{dd}^{r(0)}(t-t') &= \int dt_1 [g_d^r(t_1-t') \\ &\quad + t_L G_{d,Lk}^{r(0)}(t-t_1)g_d^r(t_1-t') \\ &\quad + t_R G_{d,Rk}^{r(0)}(t-t_1)g_d^r(t_1-t')], \end{aligned} \quad (\text{A8})$$

$$\begin{aligned} G_{dd}^{<(0)}(t-t') &= \int dt_1 [g_d^{<}(t_1-t') \\ &\quad + t_L G_{d,Lk}^{r(0)}(t-t_1)g_d^{<}(t_1-t') \\ &\quad + t_L G_{d,Lk}^{<(0)}(t-t_1)g_d^a(t_1-t') \\ &\quad + t_R G_{d,Rk}^{r(0)}(t-t_1)g_d^{<}(t_1-t') \\ &\quad + t_R G_{d,Rk}^{<(0)}(t-t_1)g_d^a(t_1-t')], \end{aligned} \quad (\text{A9})$$

where $g_d^{r(a)}(t_1-t')$ and $g_d^{<}(t_1-t')$ are the Green functions of the non-interacting electrons in an isolated dot,

$$g_d^{r(a)}(\omega) = \frac{1}{\omega - \varepsilon_0 \pm i\delta}, \quad (\text{A10})$$

$$g_d^{<}(\omega) = -2\pi i n_d \delta(\omega - \varepsilon_0). \quad (\text{A11})$$

n_d is the distribution function of electrons in the dot. By the Fourier transforms, we obtain

$$\begin{aligned} G_{dd}^{r(0)}(\omega) &= g_d^r(\omega) \\ &\quad + t_L G_{d,Lk}^{r(0)}(\omega)g_d^r(\omega) + t_R G_{d,Rk}^{r(0)}(\omega)g_d^r(\omega), \end{aligned} \quad (\text{A12})$$

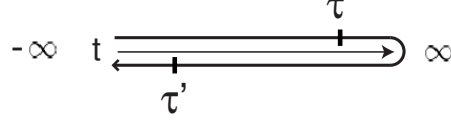


FIG. 9: Complex-time contour on which nonequilibrium-Green function theory is constructed.

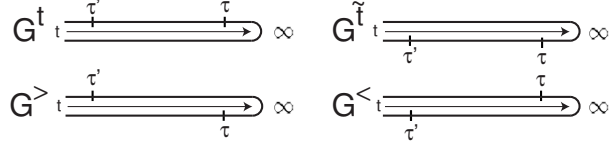


FIG. 10: Diagrams of the contour-ordered Green function $G(\tau, \tau')$. Four diagrams correspond to the real-time Green functions, G^t , $G^{\tilde{t}}$, $G^>$, and $G^<$, respectively.

$$\begin{aligned}
G_{\text{dd}}^{<(0)}(\omega) &= g_{\text{d}}^{<}(\omega) \\
&+ t_{\text{L}} G_{\text{d,Lk}}^{r(0)}(\omega) g_{\text{d}}^{<}(\omega) + t_{\text{L}} G_{\text{d,Lk}}^{<(0)}(\omega) g_{\text{d}}^a(\omega) \\
&+ t_{\text{R}} G_{\text{d,Rk}}^{r(0)}(\omega) g_{\text{d}}^{<}(\omega) + t_{\text{R}} G_{\text{d,Rk}}^{<(0)}(\omega) g_{\text{d}}^a(\omega).
\end{aligned} \tag{A13}$$

By expressing $G_{\text{d,Lk}}^{r(0)}(\omega)$, $G_{\text{d,Lk}}^{<(0)}(\omega)$, $G_{\text{d,Rk}}^{r(0)}(\omega)$, and $G_{\text{d,Rk}}^{<(0)}(\omega)$ in terms of $G_{\text{dd}}^{r(0)}(\omega)$ and $G_{\text{dd}}^{<(0)}(\omega)$, we obtain Eqs. (10) and Eq. (25).

APPENDIX B: PERTURBATION EXPANSION

We discuss elastic and inelastic processes by the e-ph interaction, using the contour-ordered Green function. The contour-ordered Green function of the quantum dot is defined as

$$G_{\text{dd}}(\tau, \tau') = -i \langle T_C \{ S d(\tau) d^\dagger(\tau') \} \rangle, \tag{B1}$$

where

$$S = T_C \left\{ \exp \left[-i \int_C d\tau_1 H_{\text{e-ph}}(\tau_1) \right] \right\} \tag{B2}$$

is the contour-ordered S matrix and $d(\tau) = e^{iH\tau} d e^{-iH\tau}$. As shown in Fig. 9, the contour path C goes from $t = -\infty$ to $t = \infty$ and goes back to $t = -\infty$.²⁹ The time labels τ and τ' are located on the contour path. The contour-ordering operator T_C orders the operators following it in contour sense: Operators with time labels later on the contour are moved left of operators of earlier time labels.

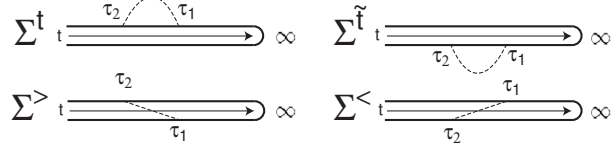


FIG. 11: Diagrams of the contour-ordered Green function with self-energies. Solid lines indicate the contour-ordered Green function of the dot electron, whereas dashed lines indicate the contour-ordered Green function of phonons. Four diagrams correspond to the real-time Green functions with self energies of Σ^t , $\Sigma^{\tilde{t}}$, $\Sigma^<$, and $\Sigma^>$, respectively.

The contour-ordered Green function, $G(\tau, \tau')$, is related to the real-time nonequilibrium Green functions, as shown in Fig. 10: $G^t(t - t')$ when τ and τ' are on the upper branch, $G^{\tilde{t}}(t - t')$ when τ and τ' are on the lower branch, and $G^>(t - t')$ [$G^<(t - t')$] when τ' is on the upper [lower] branch and τ is on the lower [upper] branch.

The contour-ordered Green function obeys Wick's theorems in the contour-time order. In the second-order perturbation with respect to the e-ph interaction,

$$G_{\text{dd}}(\tau, \tau') = G_{\text{dd}}^0(\tau, \tau') + \int_C d\tau_1 \int_C d\tau_2 G_{\text{dd}}^0(\tau, \tau_1) \Sigma(\tau_1, \tau_2) G_{\text{dd}}(\tau_2, \tau'), \quad (\text{B3})$$

$$\Sigma(\tau_1, \tau_2) = \sum_{\mathbf{q}} M_{\mathbf{q}} G_{\text{dd}}^0(\tau_1, \tau_2) D(\mathbf{q}, \tau_1, \tau_2), \quad (\text{B4})$$

where

$$G_{\text{dd}}^0(\tau_1, \tau_2) = -i \langle T_C \{ d(\tau) d^\dagger(\tau') \} \rangle_{\text{el}}, \quad (\text{B5})$$

$$D(\mathbf{q}, \tau_1, \tau_2) = -i \langle T_C Q(\tau_1) Q(\tau_2) \rangle_{\text{ph}}, \quad (\text{B6})$$

with

$$Q(\tau) = a_{\mathbf{q}}(\tau) + a_{-\mathbf{q}}^\dagger(\tau). \quad (\text{B7})$$

The bracket $\langle \ \rangle_{\text{el}}$ denotes the average over the states of dot electron in the absence of e-ph interaction and $\langle \ \rangle_{\text{ph}}$ denotes the average over those of phonons in the equilibrium state. Figure 11 shows four types of diagrams for the self-energies. Solid lines indicate the contour-ordered Green function of the dot electron, whereas dashed lines indicate the contour-ordered Green function of phonons. The diagrams can be divided into two types, one corresponds to the elastic process and the other corresponds to the inelastic process.

When τ_1 and τ_2 are on the same branch of contour path C , electrons emit (absorb) and absorb (emit) phonons. Therefore, the phonon state at $t = \infty$ is the same as at $t = -\infty$. This is the elastic process in which the energy of electrons conserves. On the other hand, when τ_1 and τ_2 are on the different branches of the path, electrons emit or absorb phonons before $t = \infty$. This process indicates the real emission or absorption of phonons and hence corresponds to the inelastic process. Thus, the processes are inelastic.

In practical calculations, we have adopted the real-time nonequilibrium Green functions. These four diagrams correspond to self-energies of real-time nonequilibrium Green functions Σ^t , $\Sigma^{\tilde{t}}$, $\Sigma^<$, and $\Sigma^>$, as labeled in Fig. 11. Note that our definition of elastic and inelastic processes differs from that in Refs. 19 and 20.

APPENDIX C: CANONICAL TRANSFORMATION

By the canonical transformation of^{20,23}

$$\bar{H} = e^s H e^{-s} \quad (\text{C1})$$

and approximation of the replacement of \bar{H}_T by H_T , we can divide the Hamiltonian into an

$$\bar{H}_{\text{el}} = [\varepsilon_0 - \sum_{\mathbf{q}} (M_{\mathbf{q}}^2 / \omega_{\mathbf{q}})] d^\dagger d + H_T + H_L + H_R \quad (\text{C2})$$

and phonon part $\bar{H}_{\text{ph}} = H_{\text{ph}}$. The retarded Green function is decoupled as

$$G_{\text{dd}}^r(t-t') = -i\theta(t-t') \langle \{ \tilde{d}(t), \tilde{d}^\dagger(t') \} \rangle_{\text{el}} \langle \tilde{X}(t) \tilde{X}^\dagger(t') \rangle_{\text{ph}}, \quad (\text{C3})$$

where

$$\tilde{d}(t) = e^{i\bar{H}_{\text{el}}t} d e^{-i\bar{H}_{\text{el}}t} \quad (\text{C4})$$

and

$$\tilde{X}(t) = e^{i\bar{H}_{\text{ph}}t} X e^{-i\bar{H}_{\text{ph}}t}. \quad (\text{C5})$$

The bracket $\langle \ \rangle_{\text{el}}$ denotes the average over the states of dot electron in the absence of e-ph interaction and $\langle \ \rangle_{\text{ph}}$ denotes the average over those of phonons in the equilibrium state.

The electron part is calculated by the equation-of-motion method [similar to Eq. (A8)] and the phonon part is calculated using Feynman disentangling.²⁸ We obtain the retarded Green function of the quantum dot

$$G_{\text{dd}}^r(t-t') = \bar{G}_{\text{dd}}^{r(\text{el})}(t-t') \bar{F}(t-t'), \quad (\text{C6})$$

where

$$\bar{G}_{\text{dd}}^{r(\text{el})}(t-t') = -i\theta(t-t') \exp\{-i[\varepsilon_0 - \sum_{\mathbf{q}} (M_{\mathbf{q}}^2/\omega_{\mathbf{q}}) - \frac{1}{4}\sqrt{\alpha T_r}\Gamma \cos \varphi]t + \tilde{\Gamma}/2t\}$$

and

$$\bar{F}(t) = \exp[-\Phi(t)], \quad (\text{C7})$$

$$\Phi(t) = \sum_{\mathbf{q}} \left(\frac{M_{\mathbf{q}}}{\omega_{\mathbf{q}}}\right)^2 [N_{\mathbf{q}}(1 - e^{i\omega_{\mathbf{q}}t})$$

$$+ (N_{\mathbf{q}} + 1)(1 - e^{-i\omega_{\mathbf{q}}t})]. \quad (\text{C9})$$

The Fourier transform of $G_{\text{dd}}^r(t-t')$ yeilds Eq. (44)

-
- ¹ A. Yacoby, M. Heiblum, D. Mahalu, and H. Shtrikman, Phys. Rev. Lett. **74**, 4047 (1995).
- ² R. Schuster, E. Buks, M. Heiblum, D. Mahalu, V. Umansky, and H. Shtrikman, Nature (London) **385**, 417 (1997).
- ³ K. Kobayashi, H. Aikawa, S. Katsumoto, and Y. Iye, Phys. Rev. Lett. **88**, 256806 (2002); Phys. Rev. B **68**, 235304 (2003).
- ⁴ Y. Aharonov and D. Bohm, Phys. Rev. **115**, 485 (1959).
- ⁵ U. Fano, Phys. Rev. **124**, 1866 (1961).
- ⁶ H. Akera, Phys. Rev. B **47**, 6835 (1993).
- ⁷ M.A. Davidovich, E.V. Anda, J. R. Iglesias, and G. Chiappe, Phys. Rev. B **55**, R7335 (1997).
- ⁸ B. R. Bulka and P. Stefanski, Phys. Rev. Lett. **86**, 5128 (2001).
- ⁹ J. König and Y. Gefen, Phys. Rev. Lett. **86**, 3855 (2001); Phys. Rev. B **65**, 045316 (2002).
- ¹⁰ W. Hofstetter, J. König, and H. Schoeller, Phys. Rev. Lett. **87**, 156803 (2001).
- ¹¹ O. Entin-Wohlman, A. Aharony, Y. Imry, Y. Levinson, and A. Schiller, Phys. Rev. Lett. **88**, 166801 (2002).
- ¹² A. Aharony, O. Entin-Wohlman, B. I. Halperin, and Y. Imry, Phys. Rev. B **66**, 115311 (2002).
- ¹³ A. Ueda, I. Baba, K. Suzuki, and M. Eto, J. Phys. Soc. Jpn. Suppl. A **72**, 157 (2003).
- ¹⁴ B. Kubala and J. König, Phys. Rev. B **65**, 245301 (2003).
- ¹⁵ B. Kubala and J. König, Phys. Rev. B **67**, 205303 (2003).
- ¹⁶ T. Nakanishi, K. Terakura, and T. Ando, Phys. Rev. B **69**, 115307 (2004).

- ¹⁷ E. V. Anda and F. Flores, *J. Phys.: Condens. Matter* **3**, 9087 (1991).
- ¹⁸ P. Hyldgaard, S. Hershfield, J. H. Davies, and J. W. Wilkins, *Ann. Phys. (N. Y.)* **236**, 1 (1994).
- ¹⁹ T. Brandes and B. Kramer, *Phys. Rev. Lett.* **83**, 3021 (1999).
- ²⁰ U. Lundin and R. H. McKenzie *Phys. Rev. B* **66**, 075303 (2002).
- ²¹ Lev G. Mourokh, N. J. M. Horing, and A. Y. Smirnov, *Phys. Rev. B* **66**, 085332 (2002).
- ²² M. Keil and H. Schoeller, *Phys. Rev. B* **66**, 155314 (2002).
- ²³ J. X. Zhu and A. V. Balatsky, *Phys. Rev. B* **67**, 165326 (2003).
- ²⁴ F. Marquardt and C. Bruder, *Phys. Rev. B* **68**, 195305 (2003).
- ²⁵ B. Dong, H. L. Cui, X. L. Lei, and N. J. M. Horing, *Phys. Rev. B* **71**, 045331 (2005).
- ²⁶ L. V. Keldysh, *Zh. Eksp. Teor. Fiz.* **47**, 1515 (1965).
- ²⁷ C. Caroli, R. Combescot, P. Nozieres, and D. Saint-James, *J. Phys. C: Solid St. Phys.* **4**, 917 (1971).
- ²⁸ G. D. Mahan, *Many-Particle Physics* (Plenum Press, New York, 1990).
- ²⁹ A.-P. Jauho, N. S. Wingreen, and Y. Meir, *Phys. Rev. B* **50**, 5528 (1994).
- ³⁰ P. K. Tien and J. R. Gordon, *Phys. Rev.* **129**, 647 (1963).
- ³¹ H. Bruus, K. Flensberg, and H. Smith, *Phys. Rev. B* **48**, 11144 (1993).